Energy Engineering

Tech Science Press

https://doi.org/10.32604/ee.2026.076467

ARTICLE

The Method of Distribution-Microgrid Collaborative Fault Recovery Considering Network Dynamic Reconfiguration

Song Gao[1], **Jiarui Wang**[2], **Yu Zhang**[1] **and Ling Jiang**[3,*]

[1]Grid Technology Center, State Grid Jilin Electric Power Research Institute, Changchun, 130021, China
[2]Science and Technology Innovation Department, State Grid Jilin Electric Power Research Institute, Changchun, 130021, China
[3]School of Electrical and Power Engineering, Hohai University, Nanjing, 211100, China

*Corresponding Author: Ling Jiang. Email: 241306020016@hhu.edu.cn

Received: 21 November 2025; Accepted: 04 January 2026; Published: 12 November 2026

ABSTRACT: This paper proposes a cooperative fault recovery method for distribution networks and microgrids considering dynamic network reconfiguration. First, an optimization model is constructed with the objectives of minimizing electricity purchase costs, voltage deviations, network losses, load shedding, and microgrid operation costs. The model thoroughly considers operational conditions, including power flow constraints, security operation constraints, and network reconfiguration constraints, within the distribution network. Second, to address the privacy protection requirements of distributed energy resources (DERs) in microgrids, a *k*-order approximation method is employed to establish an operation feasible region (OFR) model for microgrid operational flexibility resources. This model characterizes the operational characteristics of microgrids through power and energy boundary constraints. Finally, to solve the cooperative optimization problem between the distribution network and microgrids, a non-iterative solution method based on equivalent projection is proposed. This method decomposes the original problem into a distribution network-level optimization and microgrid-level subproblems, eliminating internal variables through equivalent projection technology to achieve cooperative optimization under privacy protection. Simulation results demonstrate that the proposed method can effectively achieve cooperative optimization of distribution network fault recovery and microgrid scheduling while protecting microgrid privacy information, significantly improving the economy and reliability of distribution network fault recovery.

KEYWORDS: Network reconfiguration; fault recovery; distribution-microgrid coordination; operational feasible region; equivalent projection

1 Introduction

The increasing penetration of renewable energy has introduced new challenges to distribution network fault recovery, including difficulties in coordinating distributed energy resources and heightened operational complexity [1,2]. Conventional fault recovery methods struggle to balance economic efficiency with reliability, while also suffering from issues such as inadequate privacy protection and low computational efficiency—limitations that become particularly pronounced in extreme weather scenarios.

In the field of distribution network fault restoration, Wan et al. [3] proposes a resilience-oriented, risk-averse strategy for pre-disaster allocation and post-disaster dispatch of emergency power resources, addressing computational challenges in power repair material allocation based on distributed robust optimization. Yuan et al. [4] proposes a multi-scenario distributed robust integrated planning model

Copyright © 2027 The Authors. Published by Tech Science Press. This work is licensed under a Creative Commons Attribution 4.0 International License, which permits unrestricted use, distribution, and reproduction in any medium, provided the original work is properly cited.

for distributed power generation and transmission networks considering typhoon disasters. This model simultaneously accounts for multiple uncertainties from wind power and grid failures, enhancing resilience through a more flexible approach. Zhou et al. [5] proposes a resilience-oriented distributed generation planning method for distribution grids. This approach comprehensively considers multiple extreme weather conditions, introduces a two-stage stochastic mixed-integer programming model, and enhances system resilience through distributed generation allocation and network topology reconfiguration. Chen et al. [6] proposes a collaborative optimization method for battery energy storage system configuration and active distribution network operation, achieving optimal battery storage deployment while adjusting network structure and distributed power generation output. de Assis et al. [7] introduces a distribution network switch configuration method considering distributed power, reducing costs while ensuring system reliability metrics—such as average outage duration—meet regulatory requirements during distributed power integration. Yao et al. [8] explores the role of distributed generation, line reinforcement, and microgrid construction combined with system reconfiguration in ensuring critical load supply during public safety outages. It proposes a robust mixed-integer programming model to enhance disaster resilience. Li and Li [9] presents a distribution network planning model incorporating distributed wind turbines, distributed photovoltaics, and energy storage systems to determine the optimal installation locations and capacities for distributed generation and energy storage within distribution networks. Additionally, regarding dynamic reconfiguration uncertainty modeling techniques, Wang et al. [10] proposes a distributed market-assisted restoration method for multi-energy distribution systems that accounts for the comprehensive uncertainties of typhoon disasters. It introduces an operability model for multi-energy distribution systems incorporating multiple auxiliary variables and establishes a risk-averse two-stage restoration framework to holistically address the combined uncertainties of line damage and renewable energy output. Hou et al. [11] proposes a two-layer optimization framework that transforms the traditional verification-based optimal power flow model for distribution networks into a dynamic network reconfiguration model centered on prosumers and oriented toward transactions. This aims to synergistically optimize peer-to-peer energy transactions among multiple microgrids and the optimal topology planning of distribution networks under uncertain conditions.

Regarding collaborative optimization strategies for distribution grids and microgrids, Kayal et al. [12] proposes a method to determine the topological boundaries of multiple microgrids during power outages in the main grid, aiming to restore distribution system supply. This approach seeks to enhance microgrid self-sufficiency by increasing power flows within the microgrid boundary. Mahendra et al. [13] explores the application of security-constrained optimal power flow incorporating line outage distribution factors in microgrids with renewable energy to enhance system resilience. Zhang et al. [14] proposes a cooperative game strategy based on the Nash bargaining model, achieving overall benefit maximization for the distribution-microgrid cooperative system through coordinated interaction among multiple microgrids under distribution network leadership. Zhao et al. [15] proposes a robust game-based reconstruction method for distribution-microgrid coordination, establishing a two-stage Stackelberg game model to address challenges posed by source-load uncertainties in the economic operation of new power systems. Wu et al. [16] proposes an energy management system framework based on collaborative multi-agent deep reinforcement learning, providing flexible scalability for microgrids while enhancing resilience during power outages and reducing operational costs. While cooperative operation modes between distribution grids and microgrids have been extensively studied, existing literature has yet to explore the application potential of microgrids in distribution grid fault restoration and their collaborative control mechanisms. Existing literature has proposed various distributed approaches for distribution-microgrid coordination models. Shi et al. [17] specifically conducted a comparative analysis of the objective functions, mathematical formulations, decision variables, and solution algorithms across various studies. It ultimately distilled the development path for

resilient distribution systems and outlined future research directions. Habib et al. [18] introduces a three-level hierarchical optimization framework employing a hierarchical distributed alternating direction method of multipliers to decompose the three-level optimization problem, fully embodying the core distributed nature of such models. Tang et al. [19] applies the alternating direction method of multipliers to the optimal power flow problem in multi-microgrid distribution systems. Aiming to reduce active power losses and enhance renewable energy utilization, it constructs a distributed secondary planning optimal power flow model where distribution and microgrids are treated as independent entities. Chen et al. [20] applies the alternating direction method to energy management problems in grid clusters across multiple time scales, minimizing the impact of uncertainties on the stable and economical operation of microgrid clusters. Xie et al. [21] proposes an autonomous optimization model for active distribution systems incorporating microgrids based on analytical goal cascading theory. This enables microgrids and distribution grids to autonomously allocate their unique resources, optimizing their respective operational states and economic benefits. Anvari et al. [22] introduces a distributed energy management strategy for multi-microgrid active distribution grids based on transactional energy markets. Its objective is to reduce operational costs for both active distribution grids and microgrids while enhancing privacy protection and addressing uncertainty. Li et al. [23] investigates a two-layer interactive optimization model for active distribution grids incorporating microgrids, employing a distributed solution approach to safeguard participant privacy. This underscores the critical importance of developing collaborative fault recovery methods for distribution grids and microgrids that integrate privacy protection with operational efficiency.

To address the aforementioned issues, this paper investigates a distribution-microgrid cooperative fault recovery method considering network dynamic reconfiguration. It proposes a two-layer cooperative optimization framework based on equivalent projection, achieving flexible resource aggregation under privacy protection by constructing a k-order approximate OFR model for microgrids. A collaborative optimization model incorporating multi-objective costs is established. A non-iterative solution method based on equivalent projection is employed to achieve the collaborative optimization of distribution network reconfiguration strategies and microgrid distributed resource dispatch. This ultimately yields a fault recovery solution that balances economic efficiency and safety.

The equivalent projection method adopted in this paper aggregates the flexibility of distributed energy resources within a microgrid to form an integrated operational feasible region model for the microgrid. This approach protects the privacy of internal distributed energy resources in the microgrid. Furthermore, during distribution-microgrid coordinated optimization, the microgrid only needs to submit the boundaries of its operational feasible region model, thereby avoiding complex information exchange with the distribution network. The coordinated optimal operation strategy can be determined through only a single round of information interaction without the need for repeated iterations, significantly reducing solution time and computational complexity, and enhancing the speed and efficiency of fault recovery.

2 The Distribution-Microgrid Cooperative Fault Recovery Model Considering Network Dynamic Reconfiguration

2.1 Distribution-Microgrid Cooperative Fault Recovery Model

2.1.1 Optimization Framework

To achieve cooperative fault recovery between the distribution network and microgrids, this paper constructs a two-layer optimization framework as shown in Fig. 1. Its core is the cooperative mechanism of "aggregated information uploading, optimized instruction downloading": each microgrid first aggregates the flexibility of its internal resources into an OFR model and uploads it; the distribution network dispatch

center then performs global optimization based on this and issues the optimized boundary exchange power instruction. The microgrids autonomously schedule their internal resources according to the instruction, while the distribution network simultaneously executes dynamic network reconfiguration. The two work in coordination to complete the restoration. This mechanism ensures optimization effectiveness while avoiding traditional iterative communication through single-round interaction, significantly improving restoration efficiency.

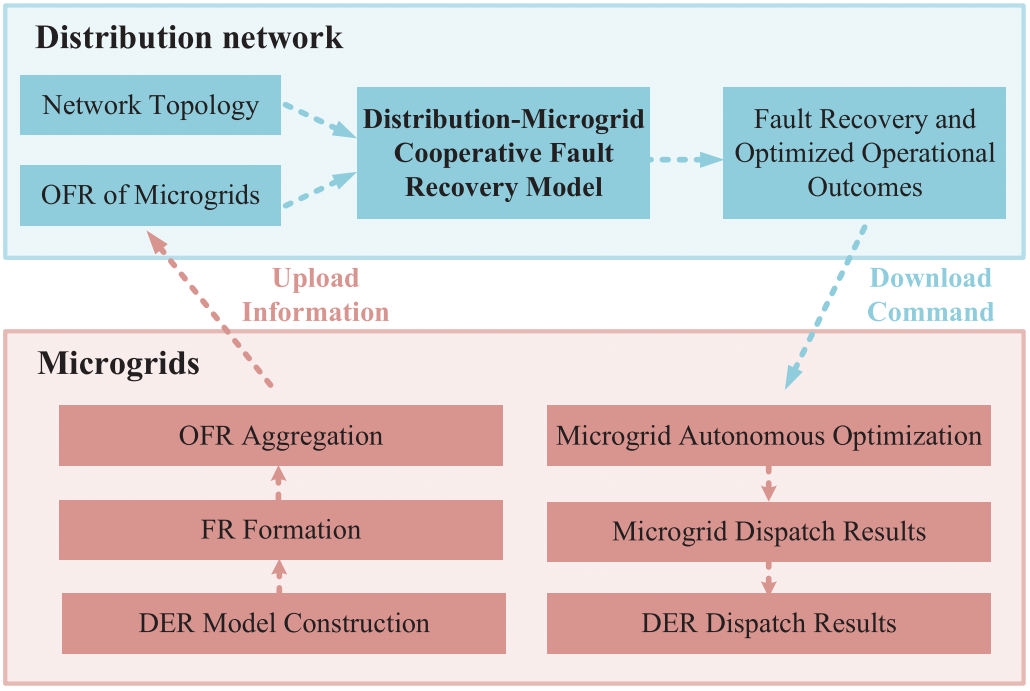


Figure 1: Framework diagram for Distribution-Microgrid cooperative fault recovery model

2.1.2 Objective Function

The Distribution-Microgrid cooperative fault recovery model aims to minimize the sum of power purchase costs, voltage deviation costs, network loss costs, load reduction costs, and microgrid operation costs. The objective function can be expressed as:

$$\min F = C_{\mathrm{DN}} + C_V + C_{loss} + C_{RE} + C_{\mathrm{MG}} \tag{1}$$

(1) Distribution network power purchase cost C_{DN}

$$C_{\mathrm{DN}} = \sum_{t=1}^{T} \sum_{n=1}^{N} c_{\mathrm{T},t} P_{\mathrm{TD}j,t} \tag{2}$$

where $c_{T,t}$ is the time-of-use price of the superior power grid; $P_{\mathrm{TD}j,t}$ is the amount of electricity purchased from the superior transmission network at the distribution network node j.

(2) Distribution network voltage deviation cost C_V

$$C_V = \sum_{t=1}^{T} \sum_{j \in DN_{bus}} c_V \left(V_{j,t} - V_{\mathrm{N}}\right)^2 \tag{3}$$

where c_V voltage deviation cost coefficient, DN_{bus} is the set of all nodes in the distribution network, $V_{j,t}$ is the voltage amplitude of node j at time t; V_N is the rated voltage, namely $V_N = 1.0$ p.u.

(3) Distribution network loss cost C_{loss}

$$C_{loss} = \sum_{t=1}^{T} \sum_{i \in DN_{bus}} \sum_{j \in v(i)} c_{loss} l_{ij,t} r_{ij} \tag{4}$$

where $v(i)$ is the set of all the end nodes with i as the initial node; c_{loss} is the cost coefficient of network loss; $l_{ij,t}$ is the square of the current amplitude flowing through the branch ij; r_{ij} is the resistance value of branch ij.

(4) Load reduction cost C_{RE}

$$C_{RE} = c_{RE} \sum_{t=1}^{T} \sum_{i \in DN_{bus}} P_{REi,t} \tag{5}$$

where c_{RE} is the load cost coefficient of the distribution network; $P_{REj,t}$ is the active load reduction of node j at time t.

(5) Microgrid operation cost C_{MG}

$$C_{MG} = \sum_{t=1}^{T} \left(\sum_{n=1}^{N} c_{D,t} P_{DMj,t} + \sum_{n=1}^{N} c_{MT} P_{MTj,t} + \sum_{n=1}^{N} c_{ESS} \left| P_{ESSj,t} \right| \right) \tag{6}$$

where $c_{D,t}$ is the time-of-use price of the distribution network; $P_{DMj,t}$ is the power purchased from the microgrid at node j to the distribution network; N is the number of microgrids; c_{MT} is the power generation cost of the gas turbine; $P_{MTj,t}$ is the active power output of the gas turbine in the access node j microgrid; c_{ESS} is the operation cost of ESS charging and discharging; $P_{ESSj,t}$ is the charging and discharging power of ESS in the access node j microgrid.

2.1.3 Distribution Network Constraints

(1) Power flow constraints of the distribution network

The power flow model of the distribution network in this paper employs the widely used branch power flow model for distribution networks. The current constraints and voltage drop constraints related to the branch model are shown in (7) and (8), respectively:

$$\left\| \begin{bmatrix} 2P_{ij,t} & 2Q_{ij,t} & l_{ij,t} - v_{i,t} \end{bmatrix}^{\mathrm{T}} \right\| \le l_{ij,t} + v_{i,t} \tag{7}$$

$$-M\left(1-\alpha_{ij,t}\right) \le v_{i,t} - v_{j,t} - 2\left(r_{ij}P_{ij,t} + x_{ij}Q_{ij,t}\right) + \left(r_{ij}^2 + x_{ij}^2\right) l_{ij,t} \le M\left(1-\alpha_{ij,t}\right) \tag{8}$$

where M is an infinite number, $\alpha_{ij,t}$ is the connected state of branch ij at time t, 1 is connected, and 0 is disconnected.

(2) Node power balance constraints

$$\sum_{i \in u(j)} \left(P_{ij,t} - l_{ij,t} r_{ij}\right) + P_{TDj,t} + P_{PVj,t} = \sum_{k \in v(j)} P_{jk,t} + P_{DLj,t} + P_{DMj,t} - P_{REj,t} \tag{9}$$

$$\sum_{i \in u(j)} \left(Q_{ij,t} - l_{ij,t} x_{ij}\right) + Q_{TDj,t} + Q_{PVj,t} = \sum_{k \in v(j)} Q_{jk,t} + Q_{DLj,t} + Q_{DMj,t} - Q_{REj,t} \tag{10}$$

where $u(j)$ is the set of all initial nodes with j as the end node; $P_{ij,t}$, $Q_{ij,t}$ are the active power and reactive power flowing through the branch ij at time t; $P_{PVj,t}$, $Q_{PVj,t}$ are the active power and reactive power injected

by the photovoltaic inverter of the distribution network to the node j of the distribution network at time t; $P_{\mathrm{DL}j,t}$, $Q_{\mathrm{DL}j,t}$ are the net active load and reactive load injected into node j at time t, respectively. $Q_{\mathrm{DM}j,t}$ is the reactive power injected by the distribution network to the access node j microgrid at time t; $Q_{REj,t}$ is the reactive load reduction of node j at time t, respectively.

(3) Safe operation constraints

The distribution network should also meet the node voltage within the safe range, and should also meet the branch current constraints, as shown in Eqs. (11) and (12):

$$v_i^{\min} \le v_{i,t} \le v_i^{\max} \tag{11}$$

$$l_{ij,t} \le l_{ij}^{\max} \tag{12}$$

where $v_i^{\max}$, $v_i^{\min}$ are the square of the maximum voltage amplitude and the square of the minimum voltage amplitude of node i, respectively, and $l_{ij}^{\max}$ is the square of the maximum current amplitude allowed to flow through the branch ij.

(4) Control constraints of the distributed photovoltaic inverter

In this paper, the optimal control model of PV inverter is adopted, which can adjust the active and reactive power output of PV inverter. The operation constraints can be obtained as follows:

$$\begin{cases} 0 \le P_{\mathrm{PV}j,t} \le P_{\mathrm{PV}j,\max} \\ P_{\mathrm{PV}j,t}^2 + Q_{\mathrm{PV}j,t}^2 \le S_{\mathrm{PV}j}^2 \\ -P_{\mathrm{PV}j,t}\sqrt{1-k_f^2}/k_f \le Q_{\mathrm{PV}j,t} \\ Q_{\mathrm{PV}j,t} \le P_{\mathrm{PV}j,t}\sqrt{1-k_f^2}/k_f \end{cases} \tag{13}$$

where $P_{\mathrm{PV}j,t}$, $Q_{\mathrm{PV}j,t}$ are the active and reactive power of the photovoltaic injection node j at time t; $P_{\mathrm{PV}j,\max}$ is the upper limit value of active power at the photovoltaic injection node j at time t; $S_{\mathrm{PV}j}$ is the rated capacity of the photovoltaic inverter at node j; $k_f = \cos\theta$ is the minimum power factor of the PV inverter, which is usually a given constant.

(5) Distribution network reconfiguration constraints

$$\beta_{ij,t} + \beta_{ji,t} = \alpha_{ij,t}, \forall ij \in DN_{branch} \tag{14}$$

$$\sum_{\substack{j \in DN_{bus} \\ j \ne i}} \beta_{ij,t} = 1, \forall i \in DN_{bus}/R \tag{15}$$

$$\sum_{\substack{j \in DN_{bus} \\ j \ne i}} \beta_{ij,t} = 0, \forall i \in R \tag{16}$$

$$\sum_{t \in T} \sum_{ij \in DN_{branch}} \left|\alpha_{ij,t} - \alpha_{ij,t-1}\right| \le \varepsilon \tag{17}$$

where $\beta_{ij,t}$ is a 0–1 variable, if the node j is the parent node of the node i, then $\beta_{ij,t}$ is 1, otherwise 0; DN_{branch} is the set of all branches of the distribution network, and R is the set of root nodes. ε is the maximum number of switching operations allowed in the network reconfiguration process during the scheduling period.

2.1.4 Microgrid Constraints

(1) Wind turbine active and reactive power output constraints

$$\begin{cases} 0 \le P_{\mathrm{WT}j,t} \le P_{\mathrm{WT}j,\max} \\ Q_{\mathrm{WT}j,\min} \le Q_{\mathrm{WT}j,t} \le Q_{\mathrm{WT}j,\max} \end{cases} \tag{18}$$

where $P_{\mathrm{WT}j,t}$, $Q_{\mathrm{WT}j,t}$ are the active and reactive power of the wind turbine injected into node j at time t; $P_{\mathrm{WT}j,\max}$ is the upper limit value of the active power at the injection node j of the wind turbine at time t; $Q_{\mathrm{WT}j,\max}$, $Q_{\mathrm{WT}j,\min}$ are the upper and lower limits of reactive power at the injection node j of the wind turbine at time t, respectively.

(2) Photovoltaic active and reactive power output constraints

Consistent with the distributed photovoltaic constraints of the distribution network, as shown in (13).

(3) Micro turbine active and reactive power output constraints

$$\begin{cases} P_{\mathrm{MT}j,\min} \le P_{\mathrm{MT}j,t} \le P_{\mathrm{MT}j,\max} \\ P_{\mathrm{MT}j,t}^2 + Q_{\mathrm{MT}j,t}^2 \le S_{\mathrm{MT}j}^2 \end{cases} \tag{19}$$

where $P_{\mathrm{MT}j,t}$, $Q_{\mathrm{MT}j,t}$ are the active and reactive power injected by the micro gas turbine to the node j through the inverter at time t; $P_{\mathrm{MT}j,\max}$, $P_{\mathrm{MT}j,\min}$ are the upper and lower limits of the active power at the micro gas turbine injection node j at time t, respectively. $S_{\mathrm{MT}j}$ is the rated capacity of the micro gas turbine inverter at node j.

(4) Energy storage system output constraint

$$\begin{cases} -P_{\mathrm{ESS}j,\max} \le P_{\mathrm{ESS}j,t} \le P_{\mathrm{ESS}j,\max} \\ P_{\mathrm{ESS}j,t}^2 + Q_{\mathrm{ESS}j,t}^2 \le S_{\mathrm{ESS}j}^2 \\ E_{\mathrm{ESS}j,t+1} = E_{\mathrm{ESS}j,t} + P_{\mathrm{ESS}j,t}\Delta t \\ E_{\mathrm{ESS}j,\max} \times 10\% \le E_{\mathrm{ESS}j,t} \le E_{\mathrm{ESS}j,\max} \times 90\% \\ E_{\mathrm{ESS}j,0} = E_{\mathrm{ESS}n,\mathrm{T}} \end{cases} \tag{20}$$

where $-P_{\mathrm{ESS}j,\max}$, $P_{\mathrm{ESS}j,\max}$ are the upper limits of the active power of the energy storage system charging and discharging at node j at time t, respectively; $P_{\mathrm{ESS}j,t}$, $Q_{\mathrm{ESS}j,t}$ are the active power and reactive power injected by the energy storage system to the node j at time t, respectively. $S_{\mathrm{ESS}j,t}$ is the maximum apparent power of node j energy storage system at time t; $E_{\mathrm{ESS}j,t}$ is the amount of electricity stored in the node j energy storage system at time t; $E_{\mathrm{ESS}j,\max}$ is the upper limit of the energy stored in the node j energy storage system at time t. In general, $E_{\mathrm{ESS}j,t}$ is set between 10% and 90% of $E_{\mathrm{ESS}j,\max}$ to protect the battery. $E_{\mathrm{ESS}j,0}$, $E_{\mathrm{ESS}j,\mathrm{T}}$ are the initial and final values of the storage capacity of the energy storage system at the node j in the scheduling period, respectively. The two are equal, which is determined by the state of charge of the energy storage system.

(5) Microgrid power balance constraints

$$P_{\mathrm{WT}j,t} + P_{\mathrm{PV}j,t} + P_{\mathrm{MT}j,t} + P_{\mathrm{ESS}j,t} + P_{\mathrm{DM}j,t} - P_{\mathrm{ML}j,t} = 0 \tag{21}$$

$$Q_{\mathrm{WT}j,t} + Q_{\mathrm{PV}j,t} + Q_{\mathrm{MT}j,t} + Q_{\mathrm{ESS}j,t} + Q_{\mathrm{DM}j,t} - Q_{\mathrm{ML}j,t} = 0 \tag{22}$$

where $P_{\mathrm{WT}j,t}$, $P_{\mathrm{PV}j,t}$, $P_{\mathrm{MT}j,t}$, $P_{\mathrm{ESS}j,t}$ are the active power output of wind power, photovoltaic, gas turbine and energy storage in the microgrid of access node j; $Q_{\mathrm{WT}j,t}$, $Q_{\mathrm{PV}j,t}$, $Q_{\mathrm{MT}j,t}$, $Q_{\mathrm{ESS}j,t}$ are the reactive power output of wind power, photovoltaic, gas turbine and energy storage in the microgrid connected to node j, respectively;

$P_{\mathrm{ML}j,t}$, $Q_{\mathrm{ML}j,t}$ are the net active load and reactive load in the microgrid connected to the node j at time t, respectively.

2.2 Microgrid OFR Model

This section aims to construct the OFR model for the microgrid to address the issue that its internal complex model cannot directly participate in the distribution network's coordinated optimization. The equivalent projection method adopted in this paper is fundamentally designed to significantly reduce computational complexity and enable rapid solution. It aggregates the high-dimensional internal model into a compact feasible region containing only boundary variables, thereby fundamentally reducing the scale of the optimization problem. Acting as a proxy, this equivalent model decouples the complex joint optimization, transforming the traditional iterative process into a "single-round interaction," which markedly enhances the overall solving speed. Concurrently, this method also protects the internal data privacy of the microgrid. The construction process will be detailed in the following text.

Due to the requirements of independent operation of power grids at all levels and privacy of user data, it is difficult to collect global information for optimal scheduling. Therefore, it is necessary to aggregate the feasible region (FR) of DER active and reactive power output in the microgrid and construct a microgrid equivalent model with privacy protection, scale reduction, and accuracy to participate in the optimal operation of the distribution network.

2.2.1 DER Monomer FR Model

The basic quantities required for modeling the DER's active and reactive power output are the maximum and minimum power that can be output, as well as the energy demand over time. In this paper, the power and energy boundary model is used to model the DER monomer FR:

$$\underline{p}_{j,t} \le p_{j,t} \le \overline{p}_{j,t} \tag{23}$$

$$\underline{e}_{j,t} \le \sum_{i=1}^{t} p_{j,i}\Delta T \le \overline{e}_{j,t} \tag{24}$$

According to the characteristics of DER, DER in microgrid can be divided into two categories. For DER with unconstrained input and output energy and unlimited time continuity of power output, it can be classified as generator-like flexibility resources, among which photovoltaics, wind turbines, and micro gas turbines belong to this kind of flexibility resources. For DERs with constraints on both input and output energy and limited time continuity of power output, they can be classified as energy storage flexibility resources, and energy storage systems are a subset of such flexibility resources.

The general form of the power and energy boundary model of generator-like flexibility resources is as follows:

$$\begin{cases} \overline{e}_{Gen,t} = \sum_{\tau=1}^{t} \overline{p}_{Gen,\tau} \\ \underline{e}_{Gen,t} = \sum_{\tau=1}^{t} \underline{p}_{Gen,\tau} \end{cases} \tag{25}$$

For energy storage-like flexible resources, the upper and lower bounds of energy over time t are derived as follows:

$$\begin{cases} \overline{e}^1_{\mathrm{ESS},t} = \min\left(\left(E_{\mathrm{ESS},0} + \overline{P}_{\mathrm{ESS},t} t\Delta T\right), 90\% E_{\mathrm{ESS,max}}\right) \\ \overline{e}^2_{\mathrm{ESS},t} = \min\left(\left(E_{\mathrm{ESS},0} + \overline{P}_{\mathrm{ESS},t}\left(T-t\right)\Delta T\right), 90\% E_{\mathrm{ESS,max}}\right) \\ \overline{e}_{\mathrm{ESS},t} = \min\left(\overline{e}^1_{\mathrm{ESS},t}, \overline{e}^2_{\mathrm{ESS},t}\right) \end{cases} \tag{26}$$

$$\begin{cases} \underline{e}^1_{\mathrm{ESS},t} = \max\left(\left(E_{\mathrm{ESS},0} + \underline{P}_{\mathrm{ESS},t} t\Delta T\right), 10\% E_{\mathrm{ESS,max}}\right) \\ \underline{e}^2_{\mathrm{ESS},t} = \max\left(\left(E_{\mathrm{ESS},0} + \underline{P}_{\mathrm{ESS},t}\left(T-t\right)\Delta T\right), 10\% E_{\mathrm{ESS,max}}\right) \\ \underline{e}_{\mathrm{ESS},t} = \max\left(\underline{e}^1_{\mathrm{ESS},t}, \underline{e}^2_{\mathrm{ESS},t}\right) \end{cases} \tag{27}$$

2.2.2 Accurate OFR Model of Microgrid

The calculation of active and reactive power OFR of microgrid is actually to calculate the Minkowski sum of G DER active and reactive power FR. The accurate OFR of microgrid containing G DER can be expressed as:

$$E_t = \sum_{g\in G} e_{g,t} \tag{28}$$

where g is the index of the DER inside the microgrid.

According to reference [24], the accurate OFR model of microgrid can be expressed as:

$$m_l \le \mathbf{a}_l^{\top}\mathbf{E} \le M_l, \forall l \in L \tag{29}$$

where $\mathbf{E} = [E_T, E_{T-1}, \ldots, E_1]^{\mathrm{T}}$, the elements in the matrix are arranged in descending order of time, L is the set of all paths of $T+1$ dimensional complete binary tree, $\mathbf{a}_l$ is a T-dimensional column vector composed of all node data on path l, which does not contain root nodes. The development trend of elements in binary tree is introduced in detail in [25].

In this paper, b_l is defined as follows:

$$b_l(t) \triangleq \sum_{\tau=1}^{t} a_l(\tau), \forall t \in [1, T]. \tag{30}$$

The following equivalent form can be obtained:

$$\mathbf{b}_l^{\top}\mathbf{P}\Delta T = \mathbf{a}_l^{\top}\mathbf{E} \tag{31}$$

Eq. (31) can be equivalently expressed as:

$$m_l \le \mathbf{b}_l^{\top}\mathbf{P}\Delta T \le M_l, \forall l \in L \tag{32}$$

According to the different parity of the number of non-zero nodes in the binary tree path, the upper and lower limits of the (32) can be calculated accordingly. When the number of non-zero nodes in the binary tree path is odd, the upper and lower limit parameter calculation formulas are:

$$M_l \triangleq \sum_{g\in G} \min\left\{\overline{e_g}(S_l) - \Delta T\left\langle \mathbf{1} - \mathbf{b}_l, \underline{\mathbf{p}_g}\right\rangle_{[s_l:r_l-1]}, \Delta T\left\langle \mathbf{b}_l, \overline{\mathbf{p}_g}\right\rangle_{[s_l:r_l-1]} + \overline{e_g}(R_l+1)\right\}. \tag{33}$$

$$m_l \triangleq \sum_{g\in G} \max\left\{\underline{e_g}(S_l) - \Delta T\left\langle \mathbf{1}-\mathbf{b}_l, \overline{\mathbf{p}_g}\right\rangle_{[s_l:r_l-1]}, \Delta T\left\langle \mathbf{b}_l, \underline{\mathbf{p}_g}\right\rangle_{[s_l:r_l-1]} + \underline{e_g}(R_l+1)\right\}. \tag{34}$$

When the number of non-zero nodes in the binary tree path is even, the upper and lower limit parameter calculation formulas are:

$$M_l \triangleq \sum_{g\in G} \min\left\{\overline{e_g}(S_l) - \underline{e_g}(R_l+1) - \Delta T\left\langle \mathbf{1}-\mathbf{b}_l, \underline{\mathbf{p}_g}\right\rangle_{[s_l:r_l-1]}, \Delta T\left\langle \mathbf{b}_l, \overline{\mathbf{p}_g}\right\rangle_{[s_l:r_l]}\right\}. \tag{35}$$

$$m_l \triangleq \sum_{g\in G} \max\left\{\underline{e_g}(S_l) - \overline{e_g}(R_l+1) - \Delta T\left\langle \mathbf{1}-\mathbf{b}_l, \overline{\mathbf{p}_g}\right\rangle_{[s_l:r_l-1]}, \Delta T\left\langle \mathbf{b}_l, \underline{\mathbf{p}_g}\right\rangle_{[s_l:r_l]}\right\}. \tag{36}$$

where $<\boldsymbol{x}, \boldsymbol{y}>_{[a:b]} = <x>_{[a:b]}^{T}.<\boldsymbol{y}>[a{:}b]$, s_l, r_l are the first and last non-zero element index on the binary tree path l, respectively. S_l and R_l are defined as follows:

$$S_l = T - s_l + 1 \tag{37}$$

$$R_l = T - r_l + 1 \tag{38}$$

Eq. (32) is the OFR exact model of the microgrid. The exact model indicates that the upper and lower limits always constrain the total energy consumed by the flexible resource cluster in each period. At the same time, it is not difficult to see from the expression that the number of constraints of the model is not related to the number of aggregated DERs, and is exponentially related to the number of layers of the complete binary tree, that is, the number of divided time periods. Excluding the invalid path with all zeros on the leftmost side of the complete binary tree, the exact OFR model contains $2^{\mathrm{T}} - 1$ valid paths with all zeros. Each path corresponds to two parameters, representing the upper and lower bounds, which account for both active and reactive power. The total number of parameters is $4(2^{\mathrm{T}} - 1)$. In the case of intra-day optimization, T is typically set to 24, and the total number of parameters can be as high as 67,108,860. The computational complexity is unacceptable.

2.2.3 The k-Order Approximation Model of Microgrid OFR

In this paper, *k*-order approximation is used to approximate the exact OFR model. This method selects the corresponding path according to the number of non-zero nodes in each path. The *k*-order approximation is to select paths with no more than k non-zero nodes to construct constraints. Therefore, the OFR model under the *k*-order approximation can be expressed as:

$$m_l \le \mathbf{b}_l^{\top}\mathbf{P}\Delta T \le M_l, \forall l \in L_k, L_k \triangleq \left\{ l \in L \left| \sum_{i=1}^{T} |a_l(i)| \le k \right.\right\} \tag{39}$$

As the approximate order increases, the calculation accuracy improves, and the computational complexity also increases. Therefore, the order of calculation should be determined according to the specific situation.

Since the microgrid aggregates the active and reactive power FR of the DER, calculates the upper and lower limits of the microgrid output and uploads it to the distribution network to participate in coordinated optimization operation, the distribution network no longer collects the specific parameters of the DER inside the microgrid, so the distribution-microgrid collaborative optimization operation model is rewritten as:

$$\min \quad C = C_{\mathrm{DN}} + C_V + C_{loss} + C_{RE} + C_{\mathrm{MG}}$$

$s.t.$ Eqs. (7)–(17) and (42) (40)

3 Non-Iterative Solution Method of Distribution-Microgrid Cooperative Model Based on Equivalent Projection

3.1 Equivalent Decomposition of Distribution-Microgrid Collaborative Optimization Model

According to the nature of the variables in the system, the decision variables in the distribution network and the microgrid are divided into coordination variables and internal variables. The distribution-microgrid collaborative optimization model can be expressed as follows:

$$\min_{x,y} F = C_{\mathrm{DN}} + C_V + C_{loss} + C_{RE} + C_{\mathrm{MG}} \tag{41}$$

$$s.t. h^D\left(x_N, y^D\right) \le 0 \tag{42}$$

$$h_n^M\left(x_n, y_n^M\right) \le 0, \forall n \in N \tag{43}$$

where $h^D(\,)$ represents the constraints of the distribution network layer; $h_n^M(\,)$ represents the constraints of the microgrid layer; n represents the index of the microgrid, and N is the set of the microgrid; x represents the coordination variable between the distribution-microgrid, such as the interaction power between the two; y represents the internal variables of the power grid, that is, the DER output in the microgrid; y^D represents the internal variable of the distribution network layer, and y_n^M represents the internal variable of the microgrid u.

For the above model, due to the presence of the coordination variable x, the distribution network layer and the microgrid layer cannot be optimized independently. If the value of x can be fixed, the joint optimization operation model can be solved hierarchically. Therefore, based on the theory of equivalent projection [26], this paper eliminates the internal variable y from the microgrid optimization model without compromising the system's optimality, and characterizes the operation characteristics of the microgrid through a set of inequality constraints on the coordination variable x. At the same time, the operating cost of the microgrid is transformed into an inequality form through the upper graph. C_n is used to represent the operating cost of the microgrid, and a variable $\overline{C}_n$ is introduced to limit the value of C_n, where any value greater than the upper bound of the operating cost $c_{3,n}$ of the microgrid can be taken. The model can be modified as:

$$\min_{x,y,C} F = C_{\mathrm{DN}} + C_V + C_{loss} + C_{RE} + \sum_{n\in N} C_n \tag{44}$$

$$s.t. h^D\left(x_N, y^D\right) \le 0 \tag{45}$$

$$h_n^M\left(x_n, y_n^M\right) \le 0, \forall n \in N \tag{46}$$

$$C_{\mathrm{MG},n} \le C_n \le \overline{C}_n, \forall n \in N \tag{47}$$

In the above model, (x_n, C_n) is used as the augmented coordination variable of microgrid n. The distribution network and microgrid are only coupled by (x_n, C_n). The internal variable y_n^M only appears in the microgrid constraints and is no longer included in the microgrid layer objective function, effectively protecting privacy information such as the microgrid layer cost.

By means of equivalent projection, the internal variable y in the original model is eliminated, and a dimensionality reduction model only about the coordination variable x and the cost variable C is constructed. The equivalent projection feasible region replaces the original model of the subsystem to participate in the optimization decision of the distribution network. It ensures that the result is equivalent to the original model.

In the above process, each microgrid submits its reduced-dimensional equivalent projection model instead of the original model to participate in the collaborative optimization operation of the distribution network layer. The collaborative optimization operation models (44)–(47) can be equivalently decomposed into the distribution network layer optimization model and the microgrid layer optimization model.

The distribution network layer optimization model is expressed as:

$$\min_{x,y^D,C} F = C_{\mathrm{DN}} + C_V + C_{loss} + C_{RE} + \sum_{n\in N} C_n \tag{48}$$

$$s.t. h^D\left(x_N, y^D\right) \le 0 \tag{49}$$

$$\left(x_n, C_n\right) \in \Pi_n, \forall n \in N \tag{50}$$

The microgrid layer optimization model is expressed as:

$$\min_{y_n^M} C_{\mathrm{MG}} = \sum_{n\in N} C_n \tag{51}$$

$$s.t. h_n^M\left(\tilde{x}_n, y_n^M\right) \le 0, \forall n \in N \tag{52}$$

$$C_n \le \tilde{C}_n, \forall n \in N \tag{53}$$

where $\tilde{x}_n$ and $\tilde{C}_n$ for the distribution network layer optimization model to solve the optimal solution.

3.2 Total Power Decomposition of Microgrid

The microgrid layer uses and as the boundary conditions to calculate the optimal solution of the internal variable y_n^M of the microgrid, that is, the optimal operating point of the microgrid. The total output of the microgrid is decomposed into the outputs of each DER. The decomposition model can be expressed as:

$$\min \delta = \left| y_n^M - \sum_{k=1}^{K} y_{n,k}^M \right|$$

$$s.t. \quad \text{Eqs. (13), (18)–(38), (52)–(53)} \tag{54}$$

where δ is the decomposition error, $y_{n,k}^M$ represents the specific output of the k-th DER in the microgrid n, and K represents the number of DERs in the microgrid. The model aims to accurately decompose the overall output power of the microgrid into the internal DERs.

4 Calculation Process of Distribution-Microgrid Collaborative Fault Recovery Method Considering Network Dynamic Reconfiguration

Combined with the established distribution-microgrid collaborative fault recovery model and the equivalent projection solution method, the specific steps of the collaborative optimization algorithm are as follows:

Step 1: Establish an optimization function with the objectives of power purchase cost, voltage deviation, network loss, load reduction and microgrid operation cost, and set the maximum number of switching operations for network reconfiguration.

Step 2: Simplify the microgrid OFR model using the k-order approximation method, calculate the active/reactive power feasible region boundary for each period, and upload it to the distribution network layer as a collaborative optimization constraint condition to facilitate information interaction while ensuring privacy protection.

Step 3: Based on the equivalent projection theory, the internal variables of the microgrid are eliminated, and a dimensionality reduction model containing only coordination variables and cost variables is constructed to form the decomposition framework of the distribution network layer optimization problem (48)–(50) and the microgrid layer sub-problem (51)–(53).

Step 4: The distribution network layer solves the optimal interactive power and cost variables based on the OFR feasible region uploaded by the microgrid, and satisfies the network reconfiguration constraints (14)–(17) and the power flow security constraints (7)–(12) to generate the switching operation scheme.

Step 5: Each microgrid uses the interactive power issued by the distribution network as the boundary condition and decomposes the total output into distributed resources, such as wind power, photovoltaic, and energy storage, through power balance constraints (21) and (22) and DER operation constraints (18)–(20).

Step 6: Check whether the reconstructed system satisfies all the constraints. If a decomposition error occurs, adjust the order of the k-order approximate model to recalculate. Otherwise, update the network topology, perform the switch operation, and output the detailed scheduling plan for each microgrid DER.

Step 7: Evaluate the effect of fault recovery, calculate performance parameters such as the comprehensive cost index, and output the optimal collaborative recovery strategy. End the process.

5 Case Study

5.1 Parameter Setting of Case Study

In this paper, the improved IEEE 33-bus test system is taken as an example. Distributed photovoltaics are connected to the distribution network nodes 7, 11, 18, 19, 27 and 33, respectively. Four microgrids are connected to the distribution network nodes 15, 22, 24 and 31, respectively. The voltage level of the distribution network is 12.66 kV, the total active load is 3715 kW, the total reactive load is 2300 kvar, the voltage amplitude of node 1 is set to 1.00 p.u., and the voltage safety range of the remaining nodes is 0.95~1.05 p.u. The system structure diagram and the load forecasting curve of the distribution network are shown in Figs. 2 and 3. The accurate OFR model of the microgrid is selected to perform an approximate calculation using the optimal approximation method, specifically a 2-order approximation, proposed in Reference [25].

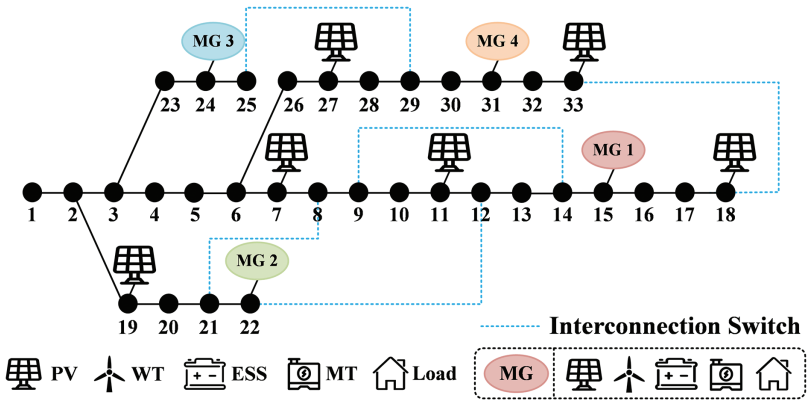


Figure 2: Structure diagram of the modified IEEE 33-node system

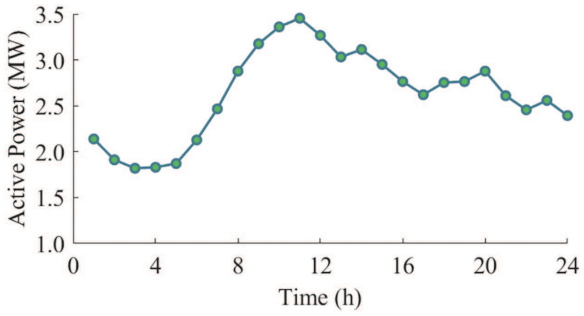


Figure 3: Load forecasting curve of the distribution network

5.2 Comparative Analysis of Optimization Results in Different Cases

Considering that permanent disconnection faults occur simultaneously in two lines between nodes 5–6 and 13–14 of the distribution network in extreme weather, the following three Cases are set to verify the effectiveness of the proposed strategy:

Case 1: The distribution network does not consider the microgrid's power network reconfiguration or the islanding of the distribution network.

Case 2: The closed part of the distribution network is connected to the switch, forming a fault recovery topology that ensures the radial operation constraints of the distribution network are met.

Case 3: Based on Case 2, the state combination of the distribution network contact switch is dynamically adjusted.

In Case 1, the distribution network is divided into three independent islanded operations due to permanent faults in the line, as shown in Fig. 4. Due to the change of power grid topology after fault isolation, the superior power grid can only provide continuous power support for island 1. In contrast, island 2 and island 3 have lost connection with the main grid. It can only rely on the autonomous operation of internal distributed photovoltaic power generation system and microgrid to maintain power supply. This operation mode significantly reduces the power purchase cost of the distribution network from the superior power grid compared to Cases 2 and 3. However, during periods of insufficient photovoltaic output, the internal power generation capacity of islands 2 and 3 cannot fully meet the load demand, resulting in the system having to take load reduction measures to maintain power balance. The amount of load reduction under Case 1 is shown in Fig. 5. These forced loads reductions result in considerable load reduction costs, which offset the benefits of reduced power purchase costs to a certain extent.

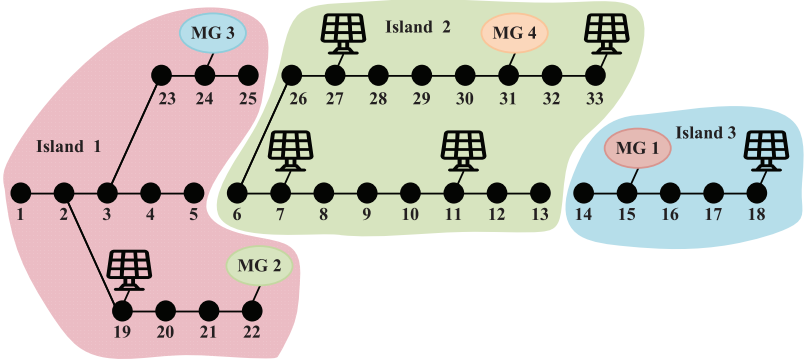


Figure 4: Islanded operation mode of the distribution network under Case 1

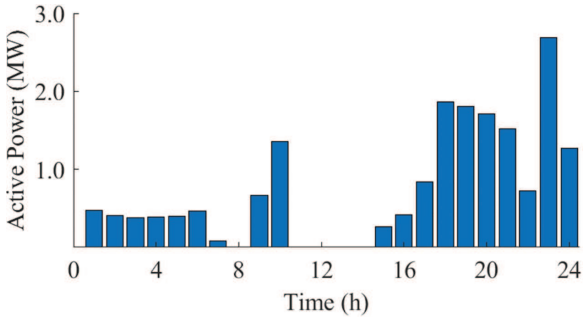


Figure 5: Load shedding amount under Case 1

The comparison of costs under the three cases is shown in Table 1. Compared with Case 1, Case 3 achieves a significant reduction in total cost by dynamically reconfiguring the distribution network topology, resulting in a savings of 5364.4 yuan (approximately 7.7%). This optimization is mainly due to the complete elimination of load reduction costs. Firstly, by eliminating the island operation mode, Case 3 completely avoids the cost of load reduction and fundamentally solves the problems of user economic loss and power supply reliability caused by power supply interruptions. Secondly, Case 3 optimizes power distribution through the coordinated operation of the main network and the microgrid, reducing the microgrid's operating cost by 924.8 yuan and the network loss cost by 809.3 yuan, which reflects the fine control ability of dynamic regulation on power flow. Compared with Case 1, Case 3 not only significantly improves the consumption capacity of renewable energy and reduces the occurrence of light abandonment, but also ensures reliable power supply throughout the day by cooperating with the main network and microgrid. It demonstrates the dual advantages of dynamic reconfiguration technology in enhancing the economic and operational reliability of distribution network operations.

Compared with Case 2, the operating cost of Case 3 is reduced by 316.2 yuan (approximately 0.5%), and the voltage fluctuation is reduced from 0.0423 to 0.0125 p.u., which is a 70.4% decrease. By dynamically adjusting the state of the tie switch, the system network loss cost is further reduced by 2.1% based on Case 2, which demonstrates that the dynamic adjustment of the tie switch can more effectively balance the power flow and suppress voltage fluctuations.

Table 1: Table of comparison of costs under different cases

Case	Cost/¥					
	C_{DN}	C_V	C_{loss}	C_{RE}	C_{MG}	Total cost
Case 1	5638.7	–	1242.3	15,102.4	47,522.0	69,505.4
Case 2	16,993.8	422.5	442.3	0	46,598.6	64,457.2
Case 3	16,985.8	125.0	433.0	0	46,597.2	64,141.0

Fig. 6 presents the voltage time-series curves for distribution network voltage weak nodes 18 and 33. The figure demonstrates that compared to Case 2, Case 3 exhibits voltage levels significantly closer to the rated value (1.0 p.u.) across all time periods and both nodes, with substantially reduced fluctuation ranges. In Case 3, the voltage at both nodes remained almost entirely within the range of 0.997 to 1.011 p.u., demonstrating excellent voltage stability. This indicates that the proposed optimization method effectively enhances the system's voltage quality throughout the entire day.

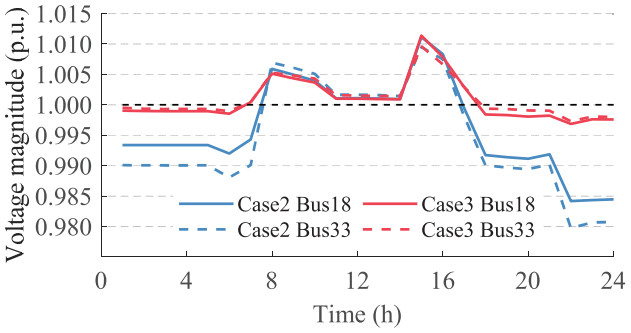


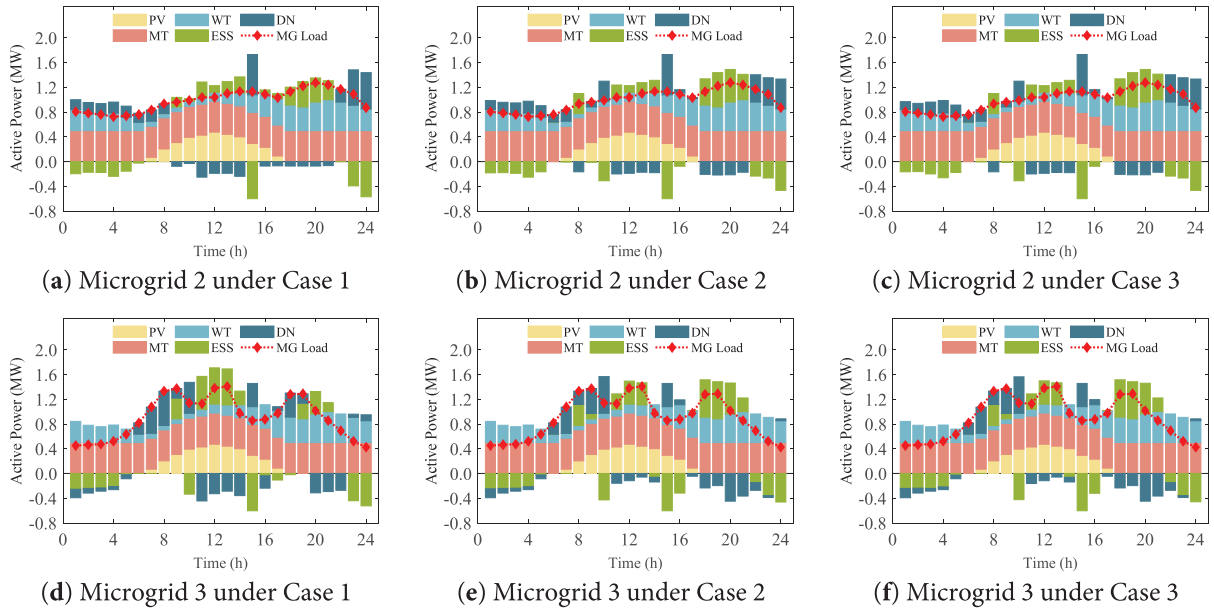
Figure 6: Voltage sequence curves at distribution network bus 18 and 33

As shown in Table 2, Case 3 achieves a comprehensive improvement in system performance by implementing a dynamic contact switch adjustment strategy, while maintaining unchanged the power supply reliability. The strategy effectively reduces the operating costs of both the main network and the microgrid by optimizing the switching state in real-time. In terms of voltage quality, the system exhibits a significant improvement, with the voltage fluctuation range accurately controlled at a better level.

Table 2: Switch operation status under Case 3

Time	Breaking branch	Action number
0:00–1:00	5–6, 13–14, 20–21, 12–22, 25–29	2
1:00–14:00	5–6, 13–14, 20–21, 18–33, 25–29	1
14:00–19:00	5–6, 13–14, 18–19, 12–22, 25–29	2
19:00–24:00	5–6, 13–14, 20–21, 18–33, 25–29	2

Fig. 7 shows the power output of Microgrids 2 and 3 under Cases 1, 2, and 3. Microgrid 2 exhibits low multi-source collaborative matching degree under Case 1: during the load valley period [0:00, 4:00), the photovoltaic output is close to zero, the gas turbine maintains a stable base output, and the energy storage mainly operates at negative power with small fluctuation amplitude. However, the power supply proportion of wind power is relatively limited, resulting in a relatively large amplitude of power interaction with the distribution network. During the load rising period [4:00, 12:00), the load gradually increases over time and the photovoltaic output starts to synchronize, but the charging-discharging switching rhythm of energy storage is not well aligned with the changes in photovoltaic output and load. In the load peak period [12:00, 15:00), the discharge power of energy storage is insufficient to effectively cover the load peak, and the distribution network has to bear additional power supply pressure. Microgrid 3 shows a consistent logical performance with Microgrid 2 under Case 1: the load rising slope is steeper, and although the wind power output increases, the output rhythm of each power source is still poorly aligned with load fluctuations, and the amplitude of power interaction with the distribution network is further expanded. This reflects the insufficient matching degree of multi-source collaborative scheduling under Case 1.



(**a**) Microgrid 2 under Case 1 (**b**) Microgrid 2 under Case 2 (**c**) Microgrid 2 under Case 3

(**d**) Microgrid 3 under Case 1 (**e**) Microgrid 3 under Case 2 (**f**) Microgrid 3 under Case 3

Figure 7: Output conditions for microgrids 2 and 3 under Cases 1, 2, and 3

Case 2 and Case 3 are highly similar and both demonstrate superior collaborative scheduling performance. For Microgrid 2 under Case 2 and Case 3, the power source coordination rhythm in each time period is basically consistent: during the load valley period [0:00, 4:00), the photovoltaic output is zero, the gas turbine provides stable power supply, wind power serves as the core basic power source, and the energy storage continuously charges at negative power, leading to a significantly narrowed amplitude of power interaction with the distribution network. During the load rising period [4:00, 12:00), the load and photovoltaic output increase synchronously, the energy storage can flexibly switch between charging and discharging modes, and the surplus photovoltaic power can be fed back to the distribution network. In the load peak period [12:00, 15:00), the energy storage discharges at high power to support the load peak. During the load fluctuation and decline phase [15:00–24:00), the energy storage dynamically adjusts its charging-discharging strategy according to load changes, resulting in minimal redundant interactive power of the distribution network. The response logic of Microgrid 3 under Case 2 and Case 3 is also highly synchronized with that of Microgrid 2 under the same cases, with only slight differences in the output amplitude of power sources during individual time periods. Overall, the collaborative performance is far superior to that of Case 1.

5.3 Comparative Analysis of Approximate Model Calculation Performance

For an accurate OFR model of a microgrid, this paper employs a k-order approximation to approximate the model. The table shows a comparison of active and reactive power decomposition errors for orders 1–3. As shown in Table 3, under the 2-order approximation, the decomposition error for both active and reactive power is very small and almost negligible, indicating that the model at this order has high accuracy. Although the complexity of the model is significantly improved compared to the 2-order approximation, the 3-order approximation makes only a minor contribution to the improvement of the decomposition error.

Table 3: Table of comparison of active and reactive power decomposition errors under different cases

Approximation order	Number of L_k	Decomposing error	
		Active power/MW	Reactive power/Mvar
1	24	13.83	4.83
2	300	10^{-10}	10^{-10}
3	2324	10^{-10}	10^{-10}

To validate the computational efficiency of the proposed method, this study compares it with the ADMM in case studies. The results are presented in Table 4. In terms of computation time, the proposed method demonstrates a significant advantage. For Cases 1 to 3, ADMM, as an iterative algorithm, requires multiple iterations to gradually approach the optimal solution. In contrast, the proposed method reduces the solution process from "hours-level" to "minutes-level," with its efficiency advantage becoming more pronounced as the problem complexity increases. The case study results indicate that, compared to traditional iterative algorithms, the proposed method achieves an order-of-magnitude improvement in efficiency for solving large-scale optimization problems due to its non-iterative solving characteristics. This provides a highly competitive new solution for practical engineering applications requiring real-time or high-frequency computation.

Table 4: Performance analysis of the proposed method in this paper

Case	Method	Number of iterations	Solution time/s
1	ADMM	37	2658
	The method in this paper (2-order)	–	90
2	ADMM	52	2963
	The method in this paper (2-order)	–	101
3	ADMM	67	4394
	The method in this paper (2-order)	–	115

6 Conclusion

Aiming to address the issue of collaborative optimization in distribution network fault recovery, this paper proposes a distribution-micro collaborative fault recovery method that considers network dynamic reconfiguration. By constructing a multi-objective optimization function, the k-order approximation is used to simplify the microgrid OFR model, and the hierarchical optimization solution is realized based on the equivalent projection theory. The verification of the improved IEEE 33-bus system demonstrates that the proposed method significantly enhances the economy and reliability of fault recovery by dynamically reconstructing the network topology, providing a new approach for the operation of smart distribution networks. The main conclusions are as follows:

The network dynamic reconfiguration strategy can significantly improve the economy and reliability of distribution network fault recovery. By dynamically adjusting the state of the contact switch, the proposed method reduces the total cost by 7.7% compared to the traditional island operation mode, while ensuring the reliability of the power supply, thereby completely eliminating the cost of load reduction. The network

dynamic reconfiguration strategy can effectively reduce the cost of network loss by 2.1% and reduce voltage fluctuation by 70.4%, which verifies the important role of dynamic reconfiguration in optimizing power flow distribution and improving voltage quality.

The collaborative optimization method of network reconfiguration based on k-order approximation achieves a good balance between computational efficiency and accuracy. The power decomposition error can be controlled to within the order of 10^{-10} MW/Mvar by using the 2-order approximation model, which greatly reduces model complexity while ensuring calculation accuracy and providing a feasible calculation framework for real-time network reconfiguration decisions.

Acknowledgement: Not applicable.

Funding Statement: This research was funded by State Grid Jilin Electric Power Company Limited Science and Technology Project: 2025-81.

Author Contributions: The authors confirm contribution to the paper as follows: Conceptualization, Song Gao and Jiarui Wang; methodology, Yu Zhang; software, Ling Jiang; All authors reviewed the results and approved the final version of the manuscript.

Availability of Data and Materials: The authors confirm that the data supporting the findings of this study are available within the article.

Ethics Approval: Not applicable.

Conflicts of Interest: The authors declare no conflicts of interest to report regarding the present study.

References

1. Shi X, Ji Y, Wang X, Tian R, Zhang C. Coordinated service restoration of integrated power and gas systems with renewable energy sources. Energy Eng. 2025;122(3):1199–220. doi:10.32604/ee.2025.061586.
2. Jain R, Velaga YN, Prabakar K, Baggu M, Schneider K. Modern trends in power system protection for distribution grid with high DER penetration. E Prime Adv Electr Eng Electron Energy. 2022;2(1):100080. doi:10.1016/j.prime.2022.100080.
3. Wan H, Liu W, Zhang S, Qie D, Shi Q, Cheng R. Pre-disaster allocation and post-disaster dispatch strategies of power emergency resources for resilience enhancement of distribution networks. Electr Power Syst Res. 2025;238(1):111038. doi:10.1016/j.epsr.2024.111038.
4. Yuan Y, Zhang H, Zhang S, Cheng H, Chen F, Wang Z, et al. A multi-scenario distributionally robust model for resilience-oriented offshore wind farms and transmission network integrated planning considering typhoon disasters. Appl Energy. 2025;392(13):125937. doi:10.1016/j.apenergy.2025.125937.
5. Zhou J, Wu X, Zhang X, Xiao F, Zhang Y, Wang X. Resilience-oriented distributed generation planning of distribution network under multiple extreme weather conditions. Sustain Energy Grids Netw. 2025;42(15):101675. doi:10.1016/j.segan.2025.101675.
6. Chen L, Jiang Y, Zheng S, Deng X, Chen H, Islam MR. A two-layer optimal configuration approach of energy storage systems for resilience enhancement of active distribution networks. Appl Energy. 2023;350(1):121720. doi:10.1016/j.apenergy.2023.121720.
7. de Assis LS, Epifanio GP, Usberti FL, González JFV, Cavellucci C. Evolutionary algorithms for switch allocation in power distribution networks with distributed generation. Electr Power Syst Res. 2025;249(1):112013. doi:10.1016/j.epsr.2025.112013.
8. Yao M, Lei S, Wu W, Callaway DS. Balancing line hardening, distributed generation and de-energization for wildfire risk mitigation with microgrid formation. Int J Electr Power Energy Syst. 2025;170(9):110842. doi:10.1016/j.ijepes.2025.110842.

9. Li H, Li L. Bilevel planning of distribution networks with distributed generation and energy storage: a case study on the modified IEEE 33-bus system. Energy Eng. 2025;122(4):1337–58. doi:10.32604/ee.2025.060105.
10. Wang Z, Hou H, Wei R, Li Z. A distributed market-aided restoration approach of multi-energy distribution systems considering comprehensive uncertainties from typhoon disaster. IEEE Trans Smart Grid. 2025;16(5):3743–57. doi:10.1109/tsg.2025.3578484.
11. Hou H, Wang Z, Zhao B, Zhang L, Shi Y, Xie C. Peer-to-peer energy trading among multiple microgrids considering risks over uncertainty and distribution network reconfiguration: a fully distributed optimization method. Int J Electr Power Energy Syst. 2023;153(2):109316. doi:10.1016/j.ijepes.2023.109316.
12. Kayal P, Maji S, Samantaray S. Assessment of topological boundaries for microgrids in an active power distribution network during emergencies. E Prime Adv Electr Eng Electron Energy. 2023;6(4):100292. doi:10.1016/j.prime.2023.100292.
13. Mahendra LS, Delfianti R, Nisa K, Mustaqim B, Harsito C, Syahroni RC. Security-constrained optimal power flow in renewable energy-based microgrids using line outage distribution factor for contingency management. Energy Eng. 2025;122(7):2695–717. doi:10.32604/ee.2025.063807.
14. Zhang Z, Shuai M, Wang B, He Y, Yang F, Ren L, et al. Cooperative game theory-based optimal scheduling strategy for microgrid alliances. Energy Eng. 2025;122(10):4169–94. doi:10.32604/ee.2025.066793.
15. Zhao R, Pan K, Lu J, Gao T, Li Y, Zhao Y, et al. A reconfiguration method of robust game for distribution-microgrid coordination considering battery aging cost. Energy Rep. 2025;13(PB):3645–60. doi:10.1016/j.egyr.2025.03.004.
16. Wu Y, Chiu WY, Tsai YP, Liu S, Hua W. Multiagent reinforcement learning in enhancing resilience of microgrids under extreme weather events. Expert Syst Appl. 2026;296(4):129145. doi:10.1016/j.eswa.2025.129145.
17. Shi Q, Liu W, Zeng B, Hui H, Li F. Enhancing distribution system resilience against extreme weather events: concept review, algorithm summary, and future vision. Int J Electr Power Energy Syst. 2022;138(15):107860. doi:10.1016/j.ijepes.2021.107860.
18. Habib S, El-Ferik S, Gulzar MM, Chauhdary ST, Ahmed EM, Alnuman H. A tri-level hierarchical optimization framework for smart homes, microgrids, and distribution networks with hydrogen integration using a distributed ADMM approach. Appl Energy. 2025;400(1):126577. doi:10.1016/j.apenergy.2025.126577.
19. Tang C, Liu M, Dai Y, Wang Z, Xie M. Decentralized saddle-point dynamics solution for optimal power flow of distribution systems with multi-microgrids. Appl Energy. 2019;252:113361. doi:10.1016/j.apenergy.2019.113361.
20. Chen L, Zhu X, Cai J, Xu X, Liu H. Multi-time scale coordinated optimal dispatch of microgrid cluster based on MAS. Electr Power Syst Res. 2019;177(5):105976. doi:10.1016/j.epsr.2019.105976.
21. Xie M, Ji X, Hu X, Cheng P, Du Y, Liu M. Autonomous optimized economic dispatch of active distribution system with multi-microgrids. Energy. 2018;153(3):479–89. doi:10.1016/j.energy.2018.04.021.
22. Anvari P, Tousi B, Talavat V, Farhadi-Kangarlu M. A smart integrated framework for resilience enhancement in distribution networks using multi-energy microgrids and distributed energy resources. Results Eng. 2025;27(3):105635. doi:10.1016/j.rineng.2025.105635.
23. Li Z, Wang H, Ai Q, Zhang Y. Interactive optimization between active distribution network with multi-microgrids based on distributed algorithm. Energy Rep. 2020;6(13):385–91. doi:10.1016/j.egyr.2020.11.226.
24. Wen Y, Hu Z, You S, Duan X. Aggregate feasible region of DERs: exact formulation and approximate models. IEEE Trans Smart Grid. 2022;13(6):4405–23. doi:10.1109/tsg.2022.3179998.
25. Wen Y, Hu Z, Liu L. Aggregate temporally coupled power flexibility of DERs considering distribution system security constraints. IEEE Trans Power Syst. 2023;38(4):3884–96. doi:10.1109/tpwrs.2022.3196708.
26. Tan Z, Yan Z, Zhong H, Xia Q. Non-iterative solution for coordinated optimal dispatch via equivalent projection: Part I: theory. IEEE Trans Power Syst. 2024;39(1):890–8. doi:10.1109/tpwrs.2023.3258066.